

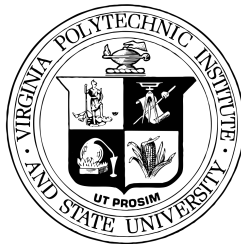
Uncertainty and Inaccuracy of Airdrop Modeling

A Thesis Presented in Partial Fulfillment of
the Honors Baccalaureate Degree in
Engineering Science and Mechanics

Thomas Magelinski

Abstract

Despite attempts to accurately model airdrop systems, predicting their landing location remains a problem. The goal of this research is to study the uncertainty and inaccuracy involved in different aspects of airdrop models in order to determine which aspects give rise to the most uncertainty. Potential sources of inaccuracy include: the complexity of parachute model, the type of wind data, and the air density model. Potential sources of uncertainty include: turbulence in the wind, and uncertainty in initial conditions. Through numerical simulation, the landing locations found using different models were compared. By holding all model aspects equal except one, the isolated effect from that single aspect is seen. It was found that the largest source of inaccuracy was the wind model. The air density model and the parachute model also had large effects on the accuracy of the landing location. The largest sources of uncertainty were the turbulence in the wind, and the release location. Based on the work in this study multiple conclusions can be drawn about why airdrop landing locations are difficult to predict and what can be done to improve operations. First, it is essential that a variable air density model be implemented, as a constant air density model was seen to be inaccurate by up to 100m. Beyond this, a model with 6 or higher degrees of freedom should be used, as the 3DoF simplification differed from the 6DoF model by up to 70m. Under a Dryden turbulence model, simulations could be expected to fall in a circle with a 60m radius. The most important result was that the wind field approximation has greater significance than the air drop system model implemented. Even when using the most accurate model considered in this study, an approximation to a fully spatiotemporally varying wind field led to inaccuracy of up to 80m.



Department of Biomedical Engineering and Mechanics
Under the supervision of Dr. Shane Ross
Virginia Polytechnic and State University
May, 2017

Contents

Abstract

Acknowledgments

1	Introduction	1
2	Description of Models	1
2.1	3DoF Isotropic Drag with Steady Fall	1
2.2	6DoF Model	2
2.3	3DoF Model Reduced from 6DoF	4
3	Z-Profiles From Simplistic Model	4
3.1	An analytical solution with no horizontal wind present.	4
3.2	Steady vertical profile only.	4
4	Inaccuracy	9
4.1	Air Density	9
4.2	Rotational Dynamics: 3DoF vs 6DoF	11
4.3	Wind Field	11
5	Uncertainty	12
5.1	Initial Conditions	12
5.2	Dryden Turbulence	13
6	Realistic Operation Analysis	14
7	Results and Conclusions	15

References

List of Figures

1	A more realistic parachute model. This model assumes a thin hemispherical shell plate as the canopy, a thin rod, massless rod connecting the canopy and the payload, and a spherical payload.	2
2	Trajectories given that the wind field has constant b values of 0.001 (a) and 0.005 (b).	5
3	Trajectories given that the wind field has constant b values of 0.01, 0.03, and 0.1	6
4	Two examples of z -profile data used to create linear approximations of how wind speed varies with height.	7
5	The dark lines represent the mean functions. The fainter lines show the function when one standard deviation is added.	8
6	Assuming a package is released at from 1500m at 65m/s it can be expected to land within the circle of the color corresponding to the operation location. The center of the circle corresponds to the packages initial ground location. Dark circles represent simulations using the mean a -function, while fainter circles use the mean function plus one standard deviation.	9
7	The trajectories for constant air density (at sea level) and variable air density are shown under average PABR conditions. The total separation at the end of the simulation is approximately 55m.	10
8	The dark lines represent the mean functions. The fainter lines show the function when one standard deviation is added.	11
9	Trajectory comparison using 3 different types of z -profiles, as well as a 3-d wind field.	12

10	Due to different initial conditions or turbulence, different simulation yield slightly different trajectories (a) and thus, landing locations (b). The parameter chosen to quantify the differences gives an area that should encompass the landing location of 95% of all airdrops.	13
11	A sample landing spread for a wind field is shown. Blue circles represent 3DoF while red represent 6DoF. The three numbers recorded for the wind field are shown in green: the 95th percentile miss distances, R1 and R2, as well as the difference between the mean landing locations, R3.	15
12	The 95 th percentile miss distance for each inaccuracy parameter is shown. Also shown is the 150m goal for the air force	16
13	The 95 th percentile miss distance for each uncertainty parameter is shown. Also shown is the 150m goal for the air force	16
14	The 95 th percentile miss distance for the most realistic ADS model under SODAR and WRF winds. The Shift, WRF, and SODAR values correspond to R3, R1, and R2 as seen in Figure 11	17

Acknowledgments

I would like to thank my research advisor and mentor, Dr. Shane Ross. I am grateful for all of the time he has spent helping me become a researcher, and for his encouragement in my academic pursuits. I would also like to thank Dr. Shibabrat Naik for his help using the computing cluster, parallelizing my simulations, and including me in the graduate research group. Lastly, I would like to thank the Department of Biomedical Engineering and Mechanics at Virginia Tech for their support and for the countless opportunities they have afforded me.

1 Introduction

The problem of predicting airdrop landing locations can be broken up into two problems: modeling inaccuracy and uncertainty. Inaccuracy comes from modeling simplifications. For this study, these include but are not limited to: only a 6DoF model, simplified wind, and use of constant air density. Uncertainty comes from stochastic effects during operation including turbulent gusts, and uncertain release conditions. This study seeks to quantify these effects in order to determine which factors play the biggest role in successfully modeling airdrop systems. Since results point to the importance of the wind field, further analysis of wind models is done. A simplified wind model is built from basic principles, and then applied to real wind data from four different locations. Each location represents a different terrain: desert, tundra, plains, and mountains. Using the average wind properties at each location, a conservative estimate for the landing area can be constructed using a simplified model. These landing areas proved to be accurate using a more accurate model under real wind conditions.

2 Description of Models

2.1 3DoF Isotropic Drag with Steady Fall

When we assume that drag is the same in all directions (we can relax this later on), the dynamic equation of motion of the body is

$$m\dot{\mathbf{u}}_b = \frac{1}{2}C\rho_a A|\mathbf{u}_w - \mathbf{u}_b|(\mathbf{u}_w - \mathbf{u}_b) + m\mathbf{g} \quad (1)$$

so

$$\dot{\mathbf{u}}_b = k|\mathbf{u}_w - \mathbf{u}_b|(\mathbf{u}_w - \mathbf{u}_b) + \mathbf{g} \quad (2)$$

where

$$k \equiv \frac{\frac{1}{2}C\rho_a A}{m} = \frac{g}{V^2}$$

where C = coefficient of drag, A = projected area of the body in any direction, \mathbf{u}_b = inertial velocity of body, \mathbf{u}_w = wind velocity, $\mathbf{g} = -g\mathbf{e}_3$ = gravity acceleration vector, ρ_a = density of air, m = mass of the body, and V = the terminal velocity.

We can non-dimensionalize this equation by scaling by the terminal velocity V , the time-scale $T = V/g$ (using $t = T\tau$), and the length-scale $L = V^2/g$,

$$\begin{aligned} \frac{d\mathbf{x}_b}{d\tau} &= \mathbf{v}_b \\ \frac{d\mathbf{v}_b}{d\tau} &= |\mathbf{v}_w - \mathbf{v}_b|(\mathbf{v}_w - \mathbf{v}_b) - \mathbf{e}_3 \end{aligned} \quad (3)$$

where $\mathbf{u}_w = V\mathbf{v}_w$ and $\mathbf{u}_b = V\mathbf{v}_b$. In these units, the terminal velocity is 1. In components, we have $\mathbf{x} = (x_1, x_2, x_3)$ and the 3D spatiotemporally varying wind field is $\mathbf{v}_w(\mathbf{x}, \tau) = (v_1(x_1, x_2, x_3, \tau), v_2(x_1, x_2, x_3, \tau), v_3(x_1, x_2, x_3, \tau))$.

Horizontal-vertical decomposition and the zero vertical wind assumption. We will decompose the motion into vertical and horizontal. We will assume that the vertical wind is zero, $v_3 = 0$, so $\mathbf{v}_w = (\mathbf{v}_w^h, 0)$, where $\mathbf{v}_w^h = (v_1, v_2)$ is the horizontal wind. We will further assume that the vertical motion has achieved a relative equilibrium at terminal velocity, so we assume that the body falls with unit speed,

$$\frac{dx_3}{d\tau} = -1$$

We will further decompose the body horizontal velocity \mathbf{v}_b^h into the wind horizontal velocity \mathbf{v}_w^h and a relative horizontal velocity $\mathbf{v}_r^h = \mathbf{v}_b^h - \mathbf{v}_w^h$, in which case we have

$$\begin{aligned} \frac{d\mathbf{x}_b^h}{d\tau} &= \mathbf{v}_r^h + \mathbf{v}_w^h \\ \frac{d\mathbf{v}_r^h}{d\tau} + \frac{d\mathbf{v}_w^h}{d\tau} &= -(|\mathbf{v}_r^h|^2 + 1)^{1/2}\mathbf{v}_r^h \end{aligned} \quad (4)$$



Figure 1: A more realistic parachute model. This model assumes a thin hemispherical shell plate as the canopy, a thin rod, massless rod connecting the canopy and the payload, and a spherical payload.

where $\mathbf{x}_b = (\mathbf{x}_b^h, x_3^0 - \tau)$ is the current location at time τ where the initial height at $\tau = 0$ is x_3^0 . Note that if $\mathbf{v}_r^h = \mathbf{0}$, then the body's horizontal motion is passive with the wind.

Note that the total derivative term $\frac{d\mathbf{v}_w^h}{d\tau}$ needs to be calculated since $\mathbf{v}_w^h(\mathbf{x}, \tau)$ changes in both space \mathbf{x} and time τ ,

$$\begin{aligned} \frac{d\mathbf{v}_w^h}{dt} &= \begin{bmatrix} \frac{\partial v_1}{\partial x_1} & \frac{\partial v_1}{\partial x_2} & \frac{\partial v_1}{\partial x_3} \\ \frac{\partial v_2}{\partial x_1} & \frac{\partial v_2}{\partial x_2} & \frac{\partial v_2}{\partial x_3} \end{bmatrix} \cdot \frac{d\mathbf{x}_b}{d\tau} + \frac{\partial \mathbf{v}_w^h}{\partial t} \\ &= \nabla^h \mathbf{v}_w^h \cdot (\mathbf{v}_r^h + \mathbf{v}_w^h) - \frac{\partial \mathbf{v}_w^h}{\partial x_3} + \frac{\partial \mathbf{v}_w^h}{\partial t} \end{aligned} \quad (5)$$

since $d\mathbf{x}_b/d\tau = (\mathbf{v}_r^h + \mathbf{v}_w^h, -1)$ and $\nabla^h \mathbf{v}_w^h$ is the horizontal gradient tensor of the horizontal wind velocity,

$$\nabla^h \mathbf{v}_w^h = \begin{bmatrix} \frac{\partial v_1}{\partial x_1} & \frac{\partial v_1}{\partial x_2} \\ \frac{\partial v_2}{\partial x_1} & \frac{\partial v_2}{\partial x_2} \end{bmatrix}$$

so the dynamic equation of motion becomes

$$\frac{d\mathbf{v}_r^h}{d\tau} = -(|\mathbf{v}_r^h|^2 + 1)^{1/2} \mathbf{v}_r^h - \nabla^h \mathbf{v}_w^h \cdot (\mathbf{v}_r^h + \mathbf{v}_w^h) + \frac{\partial \mathbf{v}_w^h}{\partial x_3} - \frac{\partial \mathbf{v}_w^h}{\partial t} \quad (6)$$

We can interpret these terms

$$\frac{d\mathbf{v}_r^h}{d\tau} = \underbrace{- (|\mathbf{v}_r^h|^2 + 1)^{1/2} \mathbf{v}_r^h}_{\text{drag relative to wind}} - \underbrace{\nabla^h \mathbf{v}_w^h \cdot (\mathbf{v}_r^h + \mathbf{v}_w^h)}_{\text{effect of horizontal wind gradient}} + \underbrace{\frac{\partial \mathbf{v}_w^h}{\partial x_3}}_{\text{vertical wind gradient}} - \underbrace{\frac{\partial \mathbf{v}_w^h}{\partial t}}_{\text{temporal wind gradient}} \quad (7)$$

2.2 6DoF Model

One of the two models used for analysis in this work is a 6DoF model. This model treats the parachute-payload system as a rigid body. The closest parachute design to a 3DoF model is a circular parachute. These parachutes are commonly used in airdrops and have isotropic drag in the horizontal direction. To develop this model, a very simple parachute-payload system is shown.

The model, which assumes a hemispherical shell as a canopy and a spherical payload, is created based on code from Numerica, and ‘‘Six-Degree-of-Freedom Model of a Controlled Circular Parachute’’ by Dobrokhodov, Yakimenko, and Junge [1]. The implementation of the model is based on ‘‘Performance Characteristics of an Autonomous Airdrop System in Realistic Wind Environments’’ by Ward, Montalvo, and

Costello [2]. The parameters used were as follows: package mass: 990kg, package radius: 1.25m, canopy mass: 50kg, canopy radius:6.185m, length: 24m. Nearly all drops had an initial height of 1500m and initial velocity of 65 m/s.

The variables x,y,z are used to represent the system's position while p,q,r represent the body frame angular velocities. The transformation matrix, T_{IB} is used to transform from the body frame to the inertial frame using the Euler angles (θ, ϕ, ψ) . Under this notation, $c_\theta \equiv \cos(\theta)$.

$$T_{IB} = \begin{bmatrix} c_\theta c_\psi & c_\theta s_\psi & -s_\theta \\ s_\phi s_\theta c_\psi - c_\phi s_\psi & s_\phi s_\theta s_\psi + c_\phi c_\psi & s_\phi c_\theta \\ c_\phi s_\theta c_\psi + s_\phi s_\psi & c_\phi s_\theta s_\psi - s_\phi c_\psi & c_\phi c_\theta \end{bmatrix} \quad (8)$$

Note that the matrix $T_{BI} \equiv T_{IB}^T$ is used to transform from the inertial frame to the body frame .

The angular velocities can be transformed to Euler angle with the following:

$$\begin{bmatrix} \dot{\phi} \\ \dot{\theta} \\ \dot{\psi} \end{bmatrix} = \begin{bmatrix} p \\ q \\ r \end{bmatrix} \quad (9)$$

The apparent velocity of the canopy is calculated as follows, where Vw is the wind vector and z_c is the distance from the system's center of gravity to the canopy.

$$\begin{bmatrix} Vac_x \\ Vac_y \\ Vac_z \end{bmatrix} = \begin{bmatrix} \dot{x} \\ \dot{y} \\ \dot{z} \end{bmatrix} + T_{IB} \begin{bmatrix} 0 \\ 0 \\ z_c \end{bmatrix} \begin{bmatrix} p \\ q \\ r \end{bmatrix} - \begin{bmatrix} Vw_x \\ Vw_y \\ Vw_z \end{bmatrix} \quad (10)$$

By replacing z_c with $-z_p$ (the distance from the system's center of gravity to the payload,) the payload's apparent velocity, Vap , is calculated with the same equation.

The apparent velocity vectors are used to find the drag on each object. The equation for drag is:

$$Fd_c = -\frac{1}{2}p_a c_c S_c ||Vac||Vac \quad (11)$$

where p_a is the air density, c_c is the drag coefficient for the canopy, S_c is the area of the canopy. Replacing the subscript c with the subscript p gives the drag equation for the payload. The coefficient of drag is obtained by smoothly interpolating between 0.8 and 0.5, based on the angle of attack.

For the rotational equations, the forces should be converted into the body frame.

$$F_c^B = T_{IB}(Fg_c + Fd_c) \quad (12)$$

The moment of inertia tensor of the system is defined as follows:

$$I_T \equiv \begin{bmatrix} I_{xx} & 0 & 0 \\ 0 & I_{yy} & 0 \\ 0 & 0 & I_{zz} \end{bmatrix}$$

By taking the sum of the forces and the sum of the moments, the following equations of motion are obtained.

$$(m_c + m_p) \begin{bmatrix} \ddot{x} \\ \ddot{y} \\ \ddot{z} \end{bmatrix} = Fg_c + Fd_c + Fg_p + Fd_p \quad (13)$$

$$I_T \begin{bmatrix} \dot{p} \\ \dot{q} \\ \dot{r} \end{bmatrix} + \begin{bmatrix} qr(I_{zz} - I_{yy}) \\ pr(I_{xx} - I_{zz}) \\ pq(I_{yy} - I_{xx}) \end{bmatrix} = \begin{bmatrix} 0 \\ 0 \\ z_c \end{bmatrix} \times F_c^B + \begin{bmatrix} 0 \\ 0 \\ -z_p \end{bmatrix} \times F_p^B \quad (14)$$

While the main parameter in the 3DoF model is the terminal velocity, the 6DoF model has many parameters. For a fair comparison, the radius of the 6DoF parachute was adjusted to 8.66m so that the average fall speed would be equal to the previously used value of 7m/s. Using the average wind at ILN plus one standard deviation (7-14m/s) the two models gave landing locations only 10m apart. When increasing the wind speed to between 9 and 20 m/s the difference in landing locations increased to about 70m.

2.3 3DoF Model Reduced from 6DoF

For comparison, the 6DoF model can be reduced to a 3DoF model. By setting all rotational terms to zero, and placing all of the ADS's mass at it's center of gravity, the 3DoF model is recovered.

$$m_{ADS} \begin{bmatrix} \ddot{x} \\ \ddot{y} \\ \ddot{z} \end{bmatrix} = Fg + Fd \quad (15)$$

3 Z-Profiles From Simplistic Model

3.1 An analytical solution with no horizontal wind present.

To get an idea of the solutions to this ODE, suppose there was no horizontal wind, $\mathbf{v}_w^h = \mathbf{0}$, but there was an initial body horizontal velocity of magnitude v_0 in a particular direction. Then the ODE becomes 1-dimensional in that initial direction, and it is

$$\frac{dv}{d\tau} = -v\sqrt{v^2 + 1} \quad (16)$$

with initial condition at $\tau = 0$ of $v(0) = v_0$, which has the analytical solution

$$v(\tau) = \frac{2Be^\tau}{B^2e^{2\tau} - 1} \quad (17)$$

where $B = \frac{1}{v_0} + \sqrt{\frac{1}{v_0^2} + 1}$. Thus, the relative horizontal velocity in the zero-wind case decays exponentially as $\tau \rightarrow \infty$ with decay time-scale 1.

3.2 Steady vertical profile only.

If we consider the case of a horizontal wind profile that varies in the vertical direction only (no horizontal or temporal variation), then the second and fourth terms in (7) are zero and the only variation from the exponential decay solution (17) is due to the third term, the vertical gradient.

If the vertical gradient happens to be zero (i.e., a constant horizontal wind velocity at all altitudes, $\mathbf{v}_w^h(x_3) = \bar{\mathbf{v}}_w^h = \text{constant}$), then the exponential decay of the relative horizontal velocity, (17), is still correct. The body horizontal velocity in that case asymptotically approaches approaches $\bar{\mathbf{v}}_w^h$.

If the vertical gradient was constant, i.e., $\frac{\partial \mathbf{v}_w^h}{\partial x_3} = a = \text{constant}$, then the relative horizontal velocity does not decay to zero, but instead to

$$v_r^* = \text{sgn}(a)\sqrt{\frac{1}{2}(-1 + \sqrt{1 + 4a^2})} \quad (18)$$

as $\tau \rightarrow \infty$. This is a result of a graphical analysis of the right hand side of

$$\frac{dv}{d\tau} = -v\sqrt{v^2 + 1} + a \quad (19)$$

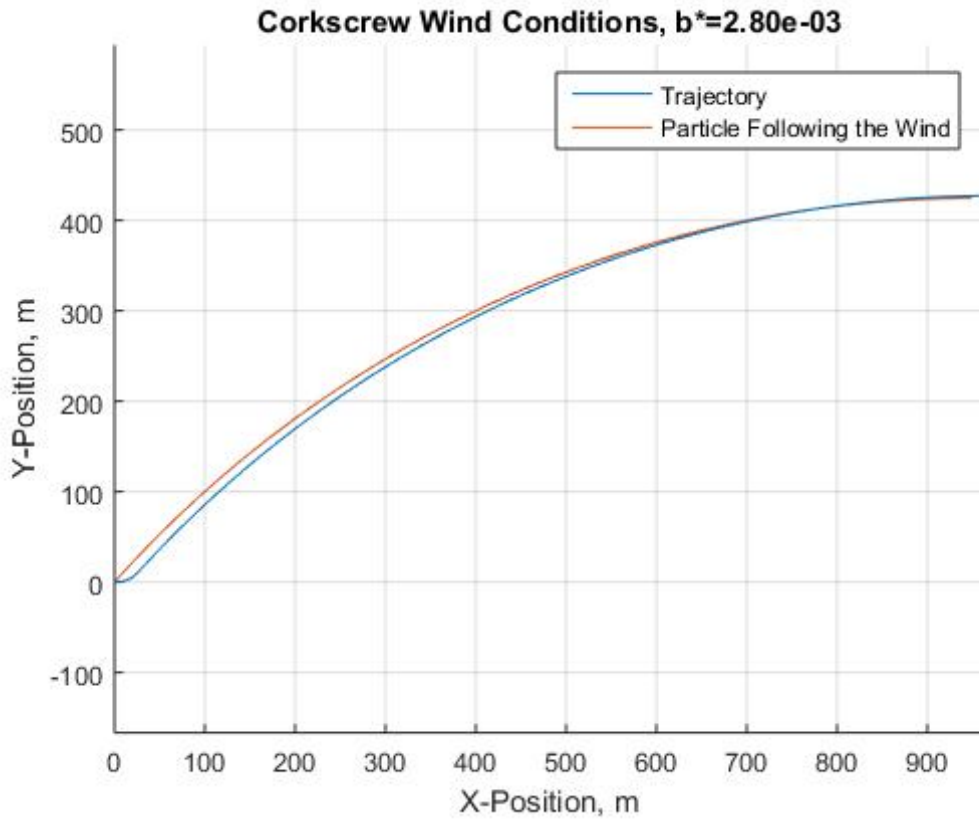
Another situation that can be considered, is a directional shear vertical profile. The magnitude of the horizontal wind velocity remains constant while the direction rotates with vertical position. This is defined by , $\mathbf{v}_w^h(x_3) = |\mathbf{v}_w^h|(\cos(b * x_3)\hat{x}_1 + \sin(b * x_3)\hat{x}_2)$ Where b is a parameter that dictates how quickly the wind field rotates with height. This will yield the equation of motion

$$\frac{d\mathbf{v}_r^h}{d\tau} = -(|\mathbf{v}_r^h|^2 + 1)^{1/2}\mathbf{v}_r^h + |\mathbf{v}_w^h|b(-\sin(b * x_3)\hat{x}_1 + \cos(b * x_3)\hat{x}_2) \quad (20)$$

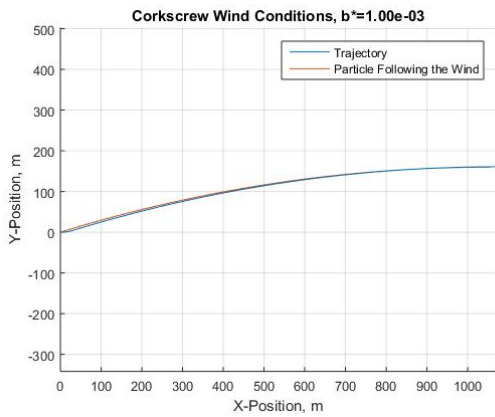
Using measured z-profile wind data, a reasonable value for b can be determined. One data set has a change in wind direction of 96° over a 3000 m elevation change. This is equivalent to a 360° rotation over the span of 11250 m. This corresponds to a b value of about 0.00054 1/m.

Through simulation, a particle trajectory governed by these equations can be compared to a particle governed by the wind. The simulation conditions for the trajectories shown are for a b value of 0.00054, a

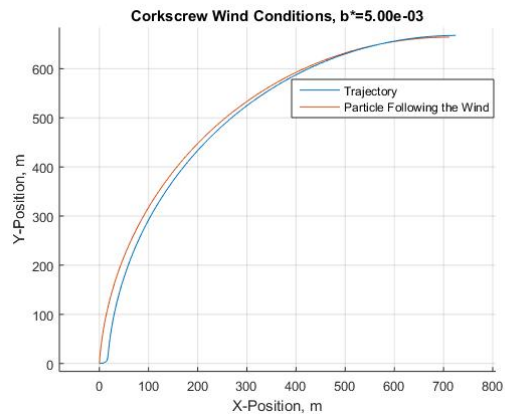
start height of 1500 m, a wind speed of 5 m/s, a terminal velocity of 7 m/s, and an initial particle speed of 65 m/s. This conditions correspond to a non-dimensional value of 0.0028.



Since a non-dimensional b value of 0.0028 is supported by wind data, it is reasonable to consider b values of 0.001 and 0.005 as well.



(a) $b=0.001$



(b) $b=0.005$

Figure 2: Trajectories given that the wind field has constant b values of 0.001 (a) and 0.005 (b).

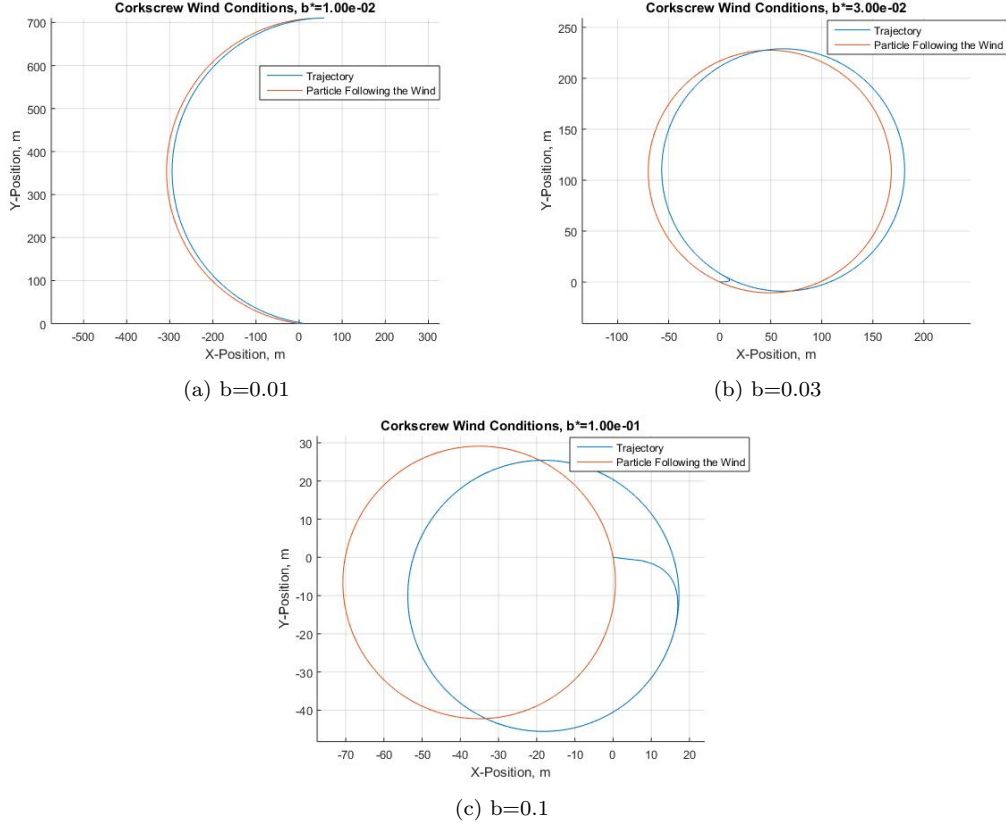


Figure 3: Trajectories given that the wind field has constant b values of 0.01, 0.03, and 0.1

Although higher order b values may be unphysical, the simulations for b values of 0.01, 0.03, and 0.1 are shown respectively due to their interesting behavior.

The radius of the circular path that the wind particle follows can be determined analytically. by taking the derivative of the velocity, acceleration can be determined to be:

$$a_w^h(t) = |\mathbf{v}_w^h| V b (\sin(bx_3(0) - bVt)\hat{x}_1 + \cos(bx_3(0) - bVt)\hat{x}_2) \quad (21)$$

Using the magnitude of the acceleration, $|a_w^h| = |\mathbf{v}_w^h| V b$, and the formula $|a_c| = \frac{|v|^2}{r}$, the radius can be found to be:

$$r = \frac{|\mathbf{v}_w^h|}{Vb} \quad (22)$$

Note that all of the acceleration is centripetal in the case of directional shear.

The constant vertical gradient situation previously discussed can be combined with the directional shear profile. This is done by introducing a horizontal wind speed function that varies linearly with height:

$$|\mathbf{v}_w^h| = \omega_0 + ax_3 \quad (23)$$

where w_0 is the wind speed at the ground. This results in the wind function:

$$\mathbf{v}_w^h(x_3) = (\omega_0 + ax_3)(\cos(b * x_3)\hat{x}_1 + \sin(b * x_3)\hat{x}_2) \quad (24)$$

The linear relationship described in equation 15 has been fitted to z-profile data from two locations, Grand Junction and Wilmington. Based on these fits, it is shown that a should be on the order of 0.001 Hz.

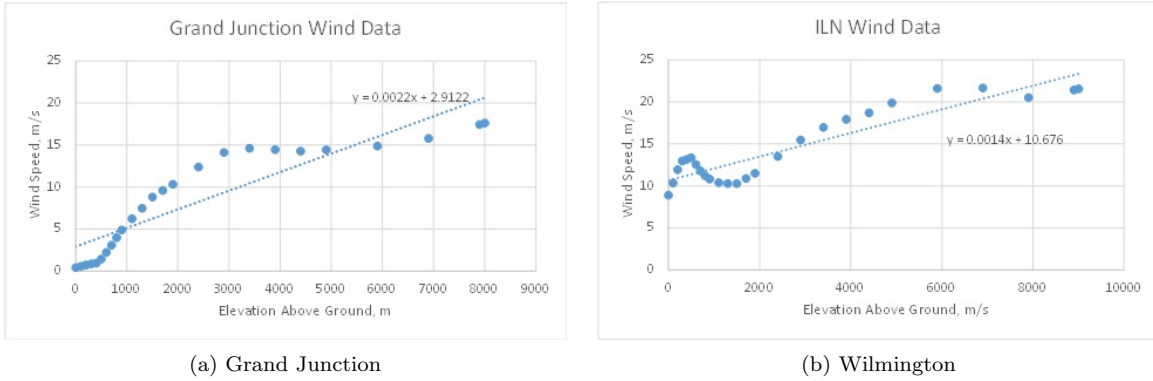
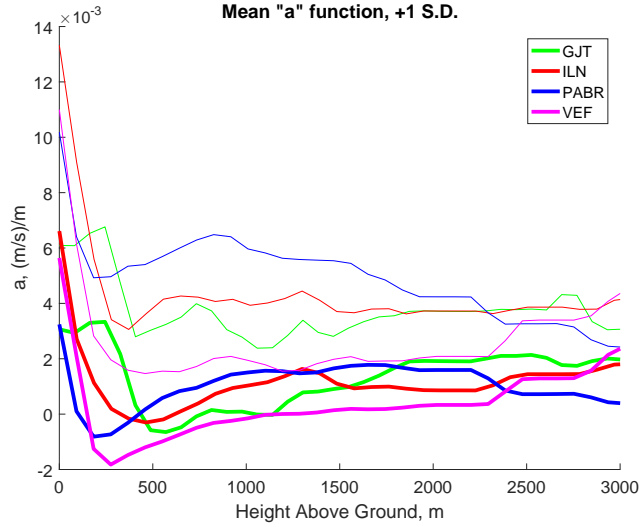
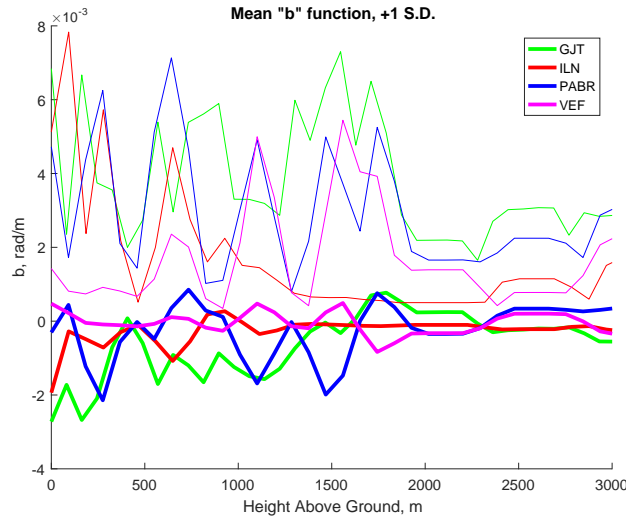


Figure 4: Two examples of z-profile data used to create linear approximations of how wind speed varies with height.

While constant a and b values can be used to approximate z-profiles constructed from data, a and b functions that vary with height can be used to recreate any z-profile exactly. Using 151 independent z-profiles across 4 different locations, typical a and b functions were found. After separating the z-profiles by location, a mean value was taken at each measured height, giving a mean function for a and b . Additionally, a standard deviation for each value was taken at each height to give an idea of variability and what higher values are reasonable. The results are shown in Figure 5.



(a) Mean a-function based on z-profile data



(b) Mean b-function based on z-profile data

Figure 5: The dark lines represent the mean functions. The fainter lines show the function when one standard deviation is added.

For each location, the mean function can be used to get an estimate of an airdrop's maximum travel distance. Increasing the a function will increase the travel distance because the wind will be higher. However, increasing the b function will decrease the maximum travel distance. This is because directional shear causes the package to follow a corkscrew trajectory. The turns in its path lead to less total distance traveled from the release point. To make the safest estimate, b must be as small as possible. Given the mean b functions shown in Figure 4, we can assume b to be zero. Also, to test a worst case scenario, the plane is assumed to be traveling in the same direction as the wind. The results are shown in Figure 6.

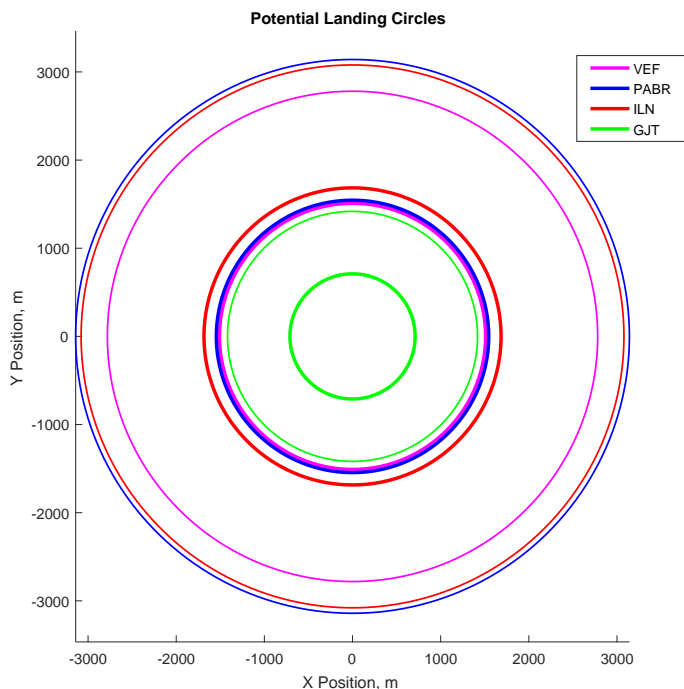


Figure 6: Assuming a package is released at from 1500m at 65m/s it can be expected to land within the circle of the color corresponding to the operation location. The center of the circle corresponds to the packages initial ground location. Dark circles represent simulations using the mean a-function, while fainter circles use the mean function plus one standard deviation.

Note that these simulations show that adding one standard deviation to the a function can vastly increase the size of the potential drop zone. Also, some locations show more variability than others. It can be expected that package will travel further at GJT than any other airport location on average. Also note that the actual wind speeds are reflected neither here nor in Figure 4. The mean ground speeds are 2.3, 7.0, 6.7, and 7.1 m/s for GJT, ILN, PABR, and VEF, respectively.

4 Inaccuracy

All modeling simplifications are sources of inaccuracy. The sources studied here are: a constant air density assumption, using a 3DoF model (vs. a 6DoF model), and using a z-profile wind (vs. a WRF wind field). These inaccuracies were tested independently via simulation over wind fields from 4 geographically distinct regions. For each wind field two simulations were run, one with the inaccurate assumption, and one with the corrected assumption. The distance between the two packages upon landing was recorded. At the end of all of the wind fields, the 95th percentile distance was taking to quantify the effect of that assumption.

4.1 Air Density

A basic assumption is that the air density is a constant, $1.225kg/m^3$, the density at sea level. This assumption is tied to the steady-fall assumption made in the 3DoF model. Without this assumption, steady fall would not occur. Thus, a variable air density is incompatible with the steady fall model, and the 3DoF model reduced from the 6DoF model must be used. The procedure to test model variable air density is outlined below. The density of air as a function of altitude can be approximated using the ideal gas law:

$$\begin{aligned}
T &= T_0 - Lh \\
p &= p_0 \left(1 - \frac{Lh}{T_0}\right)^{\frac{gM}{RL}} \\
\rho &= \frac{pM}{RT}
\end{aligned}
\tag{25}$$

Where the constants are defined as follows:

$T_0 = 288.15K$	sea level standard temperature
$p_0 = 101.325kPa$	sea level standard atmospheric pressure
$g = 9.807m/s^2$	gravitational acceleration
$L = 0.0065K/m$	temperature lapse rate
$R = 8.31447J/(molK)$	ideal gas constant
$M = 0.0289644kg/mol$	molar mass of dry air

The force of drag is directly proportional to the density of the air, so this variability is important. Of the airports with wind data, PABR has the lowest altitude (13m). Still, the ADS is dropped 1500m above ground level, so the density of air experienced is in the range $1.0567 - 1.2234kg/m^3$. Under average wind conditions at PABR, with no turbulence, a variable air density lead to a landing location 55m away from the sea level density simulation using the 6DoF model as shown in Figure 7.

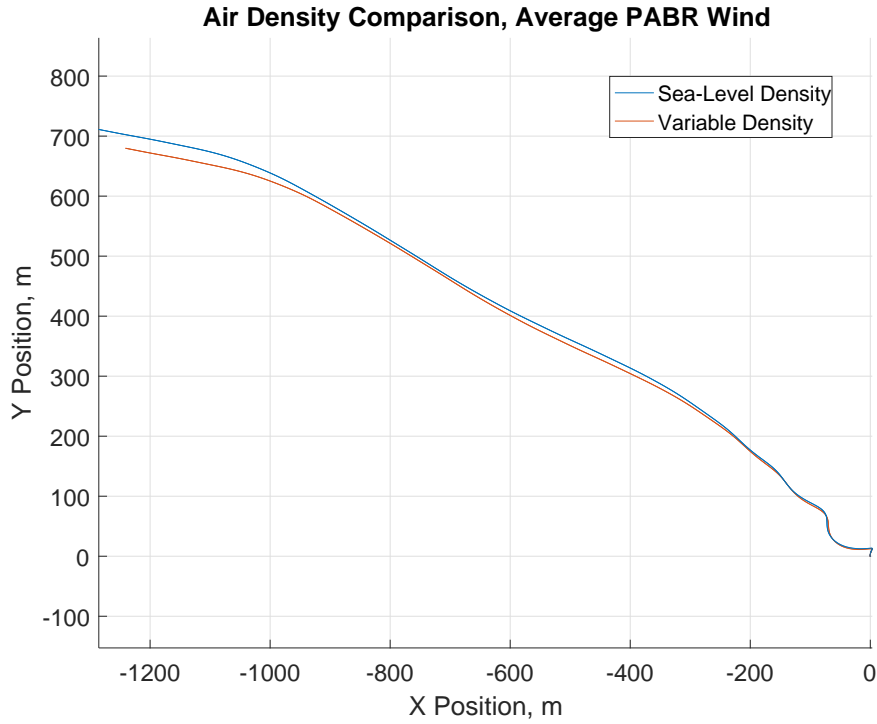


Figure 7: The trajectories for constant air density (at sea level) and variable air density are shown under average PABR conditions. The total separation at the end of the simulation is approximately 55m.

Neglecting turbulence, simulations were carried out to compare the landing location with constant and variable air densities. These simulations were run using both the 3DoF model and the 6DoF model. The 95th percentile difference is shown in Figure 12.

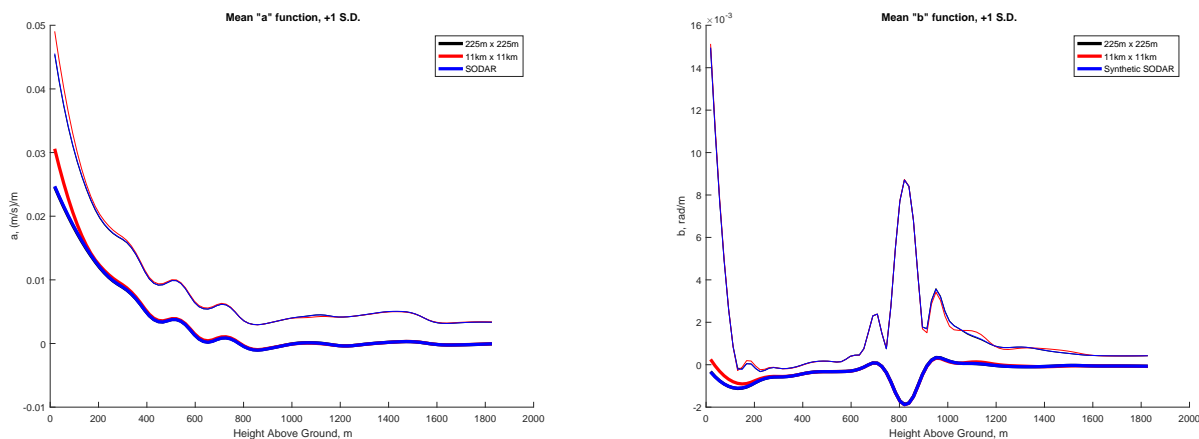
4.2 Rotational Dynamics: 3DoF vs 6DoF

A 6DoF model is a better representation of the air drop system (ADS) because of the possibility of rotation. The rotation of the system increases the drag forces, induces moments, and changes the angle of attack. Since the drag coefficient is dependent on the angle of attack, the drag coefficient is also affected by the increased degrees of freedom. A noteworthy behavior of this model is the possibility for spiraling. When given an initial rotation along the vertical axis, (the system is also initially aligned with one of the horizontal axes) the ADS will continue a small rotation about the vertical axis throughout its flight. This rotation affects the angle of attack throughout the flight which, causes the ADS to fall faster. This effect is quantified through the difference in landing locations of the 6DoF model vs that of the 3DoF model under the same conditions.

4.3 Wind Field

The wind data used for The Weather Researching and Forecasting Model (WRF Model), can be used to obtain a spatio-temporally varying wind field based on region and time. Based on the work done thus far, the question arises: How can this type of wind field best be represented in terms of a z-profile?

Three methods of conversion have been tested. The first, is to average the entire 11km by 11km space by height, and then average the result over time. The second method, is to choose a smaller region, 225m by 225m, that the drop will be preformed in and preform the same calculation. Lastly, the data from a single location on the ground closest to that of the drop location can be used from one instance of time. This last method is similar to the result obtained from using a SODAR instrument in the field, and thus, is referred to as "Synthetic SODAR." Using the same methods as were used on the z-profiles previously, the following mean a and b functions were found, and shown in Figure 8.



(a) Mean a-function based on WRF data

(b) Mean b-function based on WRF data

Figure 8: The dark lines represent the mean functions. The fainter lines show the function when one standard deviation is added.

Now, there is a larger question that can be studied: How do trajectories from z-profile wind compare to those from a WRF wind model? Knowing that the WRF model is closer to reality, if the trajectories are similar, than using z-profiles as an approximation will be confirmed as a safe assumption. If not, a source of error has been identified.

Using a single WRF field, all three z-profiles described were created. Then, simulations were run using all three z-profiles as well as the 3-dimensional wind field. All simulations began at the origin traveling at 65m/s at 1500m above the ground. The trajectories are depicted in Figure 9.

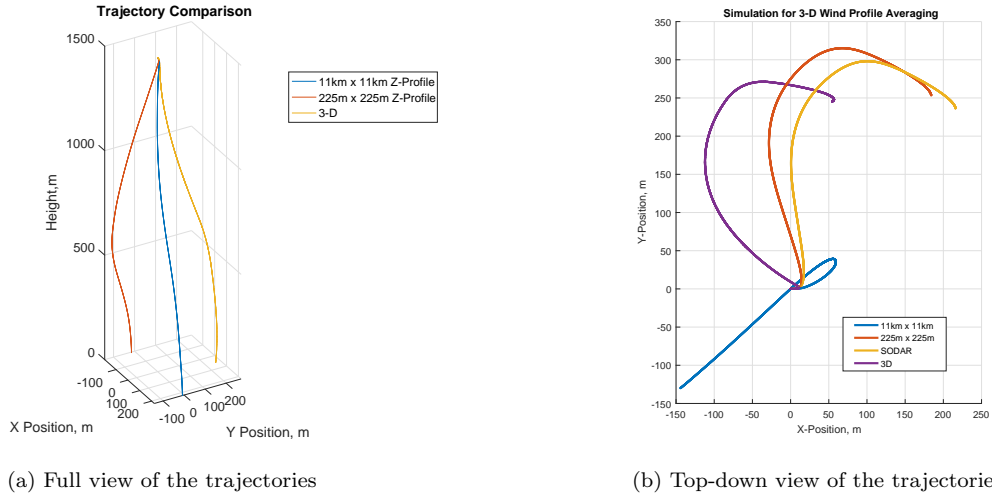


Figure 9: Trajectory comparison using 3 different types of z-profiles, as well as a 3-d wind field.

It is clear from these simulations that using the full wind field to create a z-profile yields inaccurate results. The small field averaging and the synthetic SODAR give similar results, which is aligned with how the a and b signal analysis previously done. Since their a and b functions are so similar, the results from each method do not differ significantly. While both of these z-profiles were able to get the shape of the trajectory correct, the initial direction was incorrect. This led to a landing location that was incorrect by about 175m. The scale of this inaccuracy is larger than that from other sources, and as such is of the most importance to this study. Due to the SODAR's similarity to a possible field measurement, it has been used in further simulations where WRF winds were converted to z-profiles.

5 Uncertainty

5.1 Initial Conditions

Even given a perfect model of an ADS, stochastic effects must be taken into account. In real life, two packages dropped right after one another will not land in the same exact place. The first reason for this is the release conditions and the wind turbulence. Due to the sudden nature of a parachute opening and the speed of the plane, the exact location, orientation, and angular velocity of the parachute may not be known. To study the effects of these uncertainties, Monte Carlo simulations were run using random numbers from a normal distribution with standard deviations defined as follows: 32.5m initial location, 20° initial orientation, 2.5 radians/s spiral angular velocity, and 1 radian/s rocking angular velocity. The spiral rotation corresponds to rotation about the vertical axis of the parachute, while the rocking rotation is about the axis perpendicular to that and in the direction of the initial rotation. The value of 32.5m was chosen to be the standard deviation of the initial location because it corresponds to 0.5s of uncertainty in release time, given that the initial velocity is 65m/s. A visualization of an ensemble of airdrop trajectories is shown below:

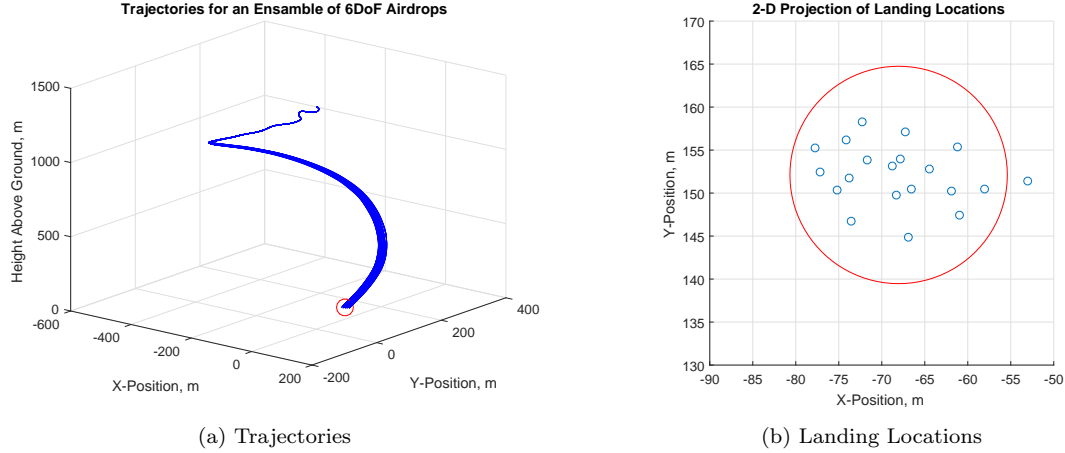


Figure 10: Due to different initial conditions or turbulence, different simulation yield slightly different trajectories (a) and thus, landing locations (b). The parameter chosen to quantify the differences gives an area that should encompass the landing location of 95% of all airdrops.

Similar to how results were found for inaccuracy effects, the 95th percentile miss distances were found from each wind field, and then again for all wind fields.

5.2 Dryden Turbulence

The second major source of uncertainty is turbulence in the wind field. For this study, a Dryden Turbulence model was used. This model filters random noise signals, η , to create stochastic gusts that are added to the deterministic wind field being used. There are three translational gusts: u_g , v_g , and w_g . The u and v gusts are added to the horizontal component, with the u -gust being added in the direction of the wind, and the v -gust being added in the direction perpendicular to the direction of the wind, CCW when looking from above. Lastly, the w -gust is added vertically. The method of Dryden Turbulence simulation was based on “Flight Data Analysis and Simulation of Wind Effects During Aerial Refueling,” by Timothy Allen Lewis [3].

The constants in the turbulence equations were designed for the U.S. Customary Units, so all parameters were converted before feeding them into the model. The resulting gust was then in ft/s, which was converted back to m/s before being fed into the rest of the model. Each gust equation is dependent on the current wind velocity, V , and on two height-dependent parameters: a spatial frequency, σ , and a length scale, L . For these equations, h is the height altitude, and W_{20} is the wind speed at 20ft above the ground. The low altitude (under 1000ft) model is shown below:

$$\begin{aligned}
 \sigma_w &= 0.1W_{20} \\
 \sigma_u = \sigma_v &= \frac{1}{(1.177 + 0.000823h)^{0.4}} \sigma_w \\
 L_w &= h \\
 L_u = L_v &= \frac{h}{(1.177 + 0.000823h)^{1.2}}
 \end{aligned} \tag{26}$$

And the high altitude (above 2000ft):

$$\begin{aligned}
 \sigma_u = \sigma_v = \sigma_w &= 0.1W_{20} \\
 L_u = L_v = L_w &= 1750
 \end{aligned} \tag{27}$$

The system of equations used to obtain the translational gusts is shown below:

$$\dot{u}_g = -\frac{V}{L_u}u_g + \sigma_u \sqrt{\frac{2V}{L_u\pi}}\eta \quad (28)$$

$$\begin{bmatrix} \dot{x}_1 \\ \dot{x}_2 \end{bmatrix} = \begin{bmatrix} 0 & 1 \\ -\frac{V^2}{L^2} & -\frac{2V}{L} \end{bmatrix} \begin{bmatrix} x_1 \\ x_2 \end{bmatrix} + \begin{bmatrix} 0 \\ \frac{V^2}{L^2} \end{bmatrix} \eta \quad (29)$$

$$v_g, w_g = \sigma \sqrt{\frac{L}{V\pi}} \left(x_1 + \sqrt{3} \frac{L}{V} x_2 \right)$$

For v_g , $\sigma = \sigma_v$ and $L = L_v$, whereas for w_g , $\sigma = \sigma_w$ and $L = L_w$.

Similarly, the Dryden turbulence model adds 3 rotational gusts to the wind field, which enter the parachute model through the angular velocity used to calculate drag. These gusts, p , q , and r correspond to rotational gusts around the u, v, and w axis, respectively. They are dependent on the size of the object moving through the wind field through the parameter b, which is here defined as the parachute's diameter. The rotational turbulence equations are shown below:

$$\dot{p}_g = \frac{V\pi}{4b} \left(-p_g + \frac{\sigma_w}{L_w^{1/3}} \sqrt{\frac{0.8}{V}} \left(\frac{\pi}{4b} \right)^{1/6} \eta \right) \quad (30)$$

$$\begin{bmatrix} \dot{x}_1 \\ \dot{x}_2 \\ \dot{x}_3 \end{bmatrix} = \begin{bmatrix} 0 & 1 & 0 \\ 0 & 0 & 1 \\ -\frac{\pi V^3}{L^2 ab} & -\frac{\pi V^2}{L^2 ab} \left(\frac{ab}{\pi} + 2L \right) & -\frac{\pi V}{Lab} \left(\frac{2ab}{\pi} + L \right) \end{bmatrix} \begin{bmatrix} x_1 \\ x_2 \\ x_3 \end{bmatrix} + \begin{bmatrix} 0 \\ 0 \\ \frac{\pi V^3}{L^2 ab} \end{bmatrix} \eta \quad (31)$$

$$q_g, r_g = \sigma \sqrt{\frac{L}{V^3\pi}} \left(x_2 + \sqrt{3} \frac{L}{V} x_3 \right)$$

For q_g , $\sigma = \sigma_w$, $L = L_w$, and $a = 4$, whereas for r_g , $\sigma = \sigma_v$, $L = L_v$, and $a = 3$.

It is important to note the instability of the model as the wind velocity reaches zero. This is due to the velocity term found in the denominator. To combat this issue during simulation, a minimum wind threshold was set to 0.3 ft/s. This threshold was found through iteration.

6 Realistic Operation Analysis

The previous analysis points to the wind model as the biggest source of error. Therefore it is of interest to see what impact the wind model may have on a more realistic airdrop scenario. In a real airdrop scenario, it is possible to take a SODAR measurement, which would yield a z-profile wind field. To study the error that this simplification leads to, the most realistic parachute model discussed was used: the 6DoF model with translational and rotational Dryden turbulence, with variable air density.

For the first set of simulations, the full WRF wind fields were used. In each field, an ensemble of 50 airdrops were performed, yielding a spread as shown in the uncertainty analysis. This spread was again quantified by the 95th percentile miss distance from the mean landing location.

For the second set of simulations, a simulated SODAR measurement was taken by recording the z-profile at the drop location at the first instance in time. As with the other z-profile tests, horizontal homogeneity was assumed. Again, 50 airdrops were performed. The 95th miss distance of this spread was also recorded. The final measurement taken for each wind field was the distance between the mean landing location under each wind field. A visualization of the three numbers that were recorded can be seen below in Figure 11.

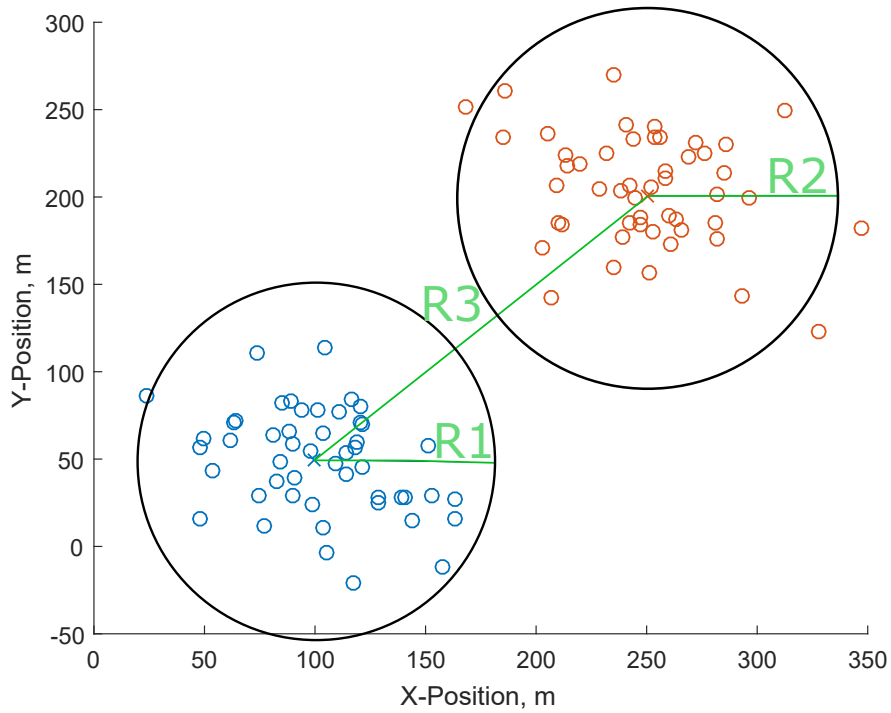


Figure 11: A sample landing spread for a wind field is shown. Blue circles represent 3DoF while red represent 6DoF. The three numbers recorded for the wind field are shown in green: the 95th percentile miss distances, R1 and R2, as well as the difference between the mean landing locations, R3.

7 Results and Conclusions

The majority of the quantitative results from this work can be summarized in Figures 12,13, and In order to estimate what types of distances are significant, a 150m benchmark line has been added. This is a goal set by the United States Air Force for the accuracy of their airdrops. While all miss distances graphed are below this line, they are isolated effects. In a real environment, these effects add onto one another, and easily surpass the 150m accuracy goal.

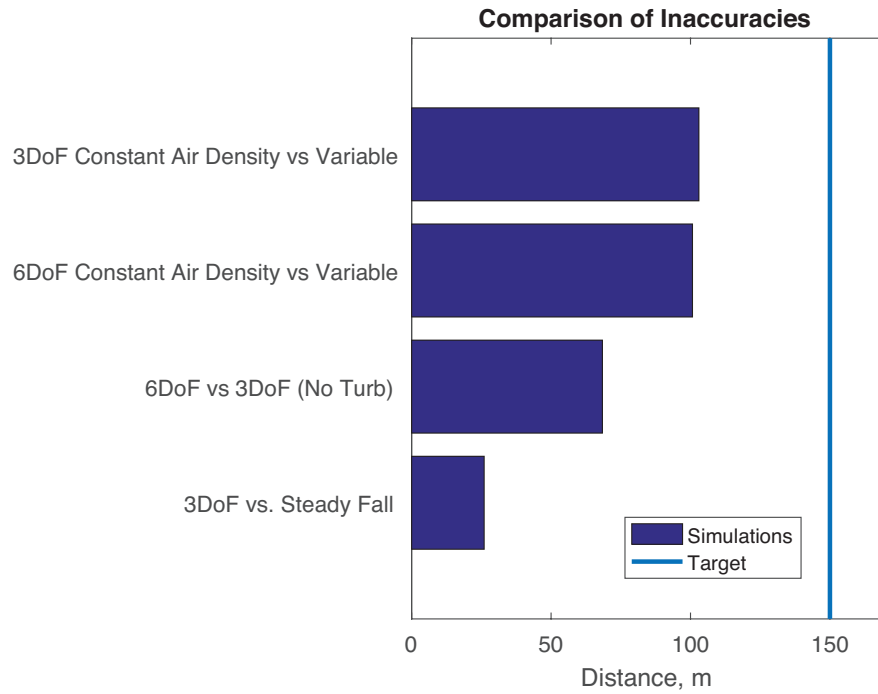


Figure 12: The 95th percentile miss distance for each inaccuracy parameter is shown. Also shown is the 150m goal for the air force

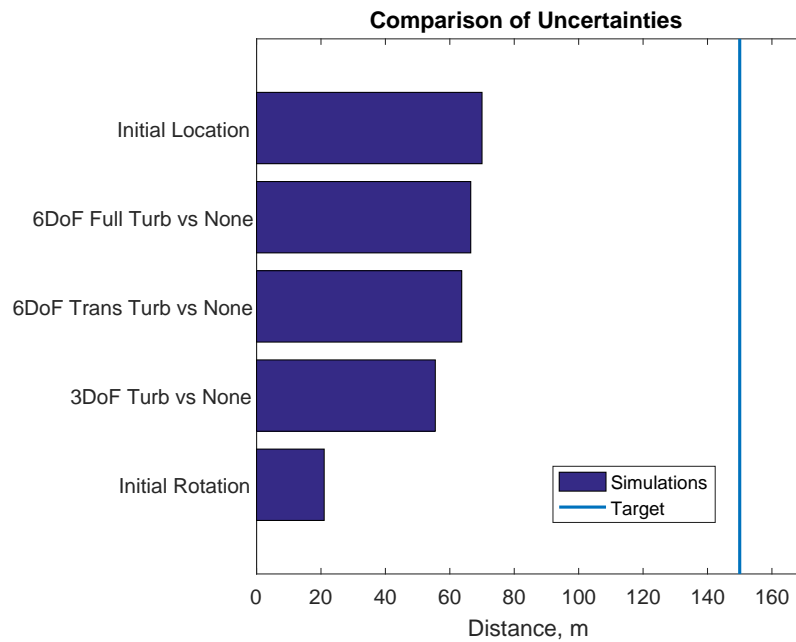


Figure 13: The 95th percentile miss distance for each uncertainty parameter is shown. Also shown is the 150m goal for the air force

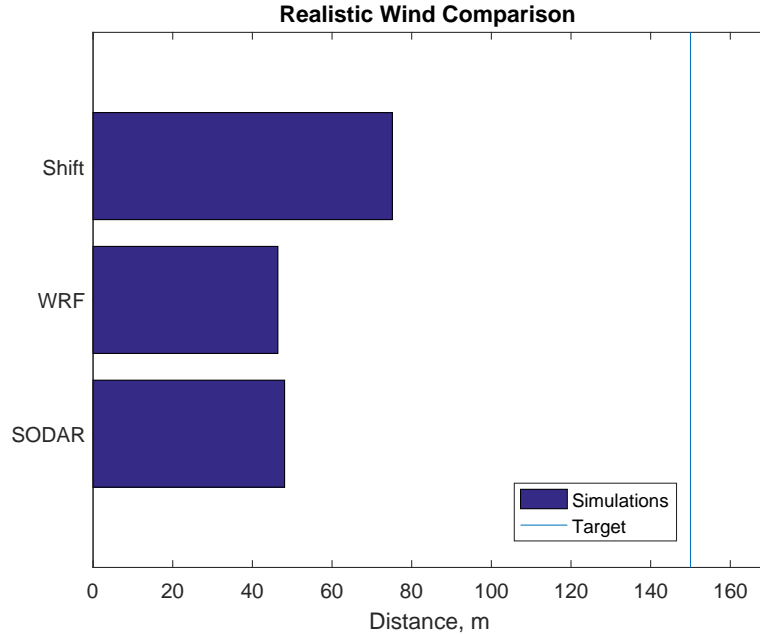


Figure 14: The 95th percentile miss distance for the most realistic ADS model under SODAR and WRF winds. The Shift, WRF, and SODAR values correspond to R3, R1, and R2 as seen in Figure 11

Inaccuracy The largest source of inaccuracy tested was the constant air density. For both the 3DoF and the 6DoF model, the 95th percentile miss distance due to air density was over 100m. Following this, comes the rotational effects captured in the 6DoF model that were not captured in the 3DoF model, which had a 95th percentile miss distance of about 70m. Lastly, the “Steady Fall” model had a 95th percentile miss distance of about 25m. As was said earlier, these effects could be combined. For example, a 3DoF Model with a constant air density may be predicted to land 170m away from a simulation of the 6DoF model with variable air density.

Uncertainty The largest source of uncertainty was the initial location. Due to the high speed of the plane, a one second difference in drop time corresponds to a 65m difference in initial location, which directly relates to the difference in landing location. After this, the full Dryden turbulence model provides the most uncertainty, with a 95th percentile miss distance of about 60m. The rotational terms in the turbulence only extended the miss distance about 5 meters. Thus, to cut down on simulation run time without sacrificing too much landing location accuracy, one might only include translational turbulence. The effect of translational turbulence on the 3DoF model was significantly less than that on the 6DoF model, by about 10m. This is again due to the rocking motion that may be induced in the 6DoF model, which cannot be induced in the 3DoF model. By sending the parachute into a spiral or rocking behavior, the spread of landing locations can be increased. Lastly, the 95th percentile miss distance due to uncertainty in the initial rotation of the ADS was calculated to be 20m.

Realistic Operation Analysis The results from the realistic operation analysis are displayed in Figure 14. This chart shows the uncertainty using both the WRF field and the SODAR field, as well as the inaccuracy caused by the SODAR approximation. The difference in uncertainty between a WRF wind field and its SODAR approximation is less than 3m, which is negligibly small compared to the scales of other uncertainties and inaccuracy. The shift between the two wind fields, however, is very large, at about 75m. This is the greatest miss distance observed in the study. Again, these distances can add together in a worst-case scenario. One simulation under a SODAR wind field may land 170m away from a single simulation under the full WRF field.

Conclusions Based on the work in this study multiple conclusions can be drawn about why airdrop landing locations are difficult to predict and what can be done to improve operations. First, it is essential that a variable air density model be implemented, as a constant air density model was seen to be inaccurate by up to 100m. Beyond this, a model with 6 or higher degrees of freedom should be used, as the 3DoF simplification differed from the 6DoF model by up to 70m. The largest source of uncertainty was found to be the initial location, due to the high speed of the plane. Unlike turbulence and initial rotation, this is fixable problem through a precise release time. Under a Dryden turbulence model, simulations could be expected to fall in a circle with a 60m radius. It was found that the rotational components to Dryden turbulence did not have a considerable impact on landing location. Furthermore, uncertainty in initial rotation accounted for 20m of uncertainty. The most important result, was that despite ADS modeling efforts, the most important factor was the wind field used. Even when using the most accurate model considered in this study, an approximation to a fully spatiotemporally varying wind field led to inaccuracy of up to 80m. From these results, the following recommendations can be made regarding airdrop modeling and operation:

1. Obtain the most accurate wind data possible, WRF model preferred.
2. Release airdrops at a very precise point.
3. Do not include rotational turbulence terms for speed of simulation.
4. Use a variable air density.
5. Estimate uncertainty along with landing location.

References

- [1] Vladimir Dobrokhodov, Oleg Yakimenko, and Christopher Junge. Six-degree-of-freedom model of a controlled circular parachute. *Journal Of Aircraft*, 40(3), 2003.
- [2] Michael Ward, Carlos Montalvo, and Mark Costello. Performance characteristics of an autonomous airdrop system in realistic wind environments. *AIAA Atmospheric Flight Mechanics Conference*, 2010.
- [3] Timothy Allen Lewis. Flight data analysis and simulation of wind effects during aerial refueling. Master's thesis, The University of Texas at Arlington, 2008.